TOPOLOGICAL MATTER

Absence of evidence for chiral Majorana modes in quantum anomalous Hall-superconductor devices

Morteza Kayyalha^{1*}, Di Xiao^{1*}, Ruoxi Zhang^{1*}, Jaeho Shin¹, Jue Jiang¹, Fei Wang¹, Yi-Fan Zhao¹, Run Xiao¹, Ling Zhang¹, Kajetan M. Fijalkowski^{2,3}, Pankaj Mandal^{2,3}, Martin Winnerlein^{2,3}, Charles Gould^{2,3}, Qi Li¹, Laurens W. Molenkamp^{2,3}, Moses H. W. Chan¹†, Nitin Samarth¹†, Cui-Zu Chang¹†

A quantum anomalous Hall (QAH) insulator coupled to an s-wave superconductor is predicted to harbor chiral Majorana modes. A recent experiment interprets the half-quantized two-terminal conductance plateau as evidence for these modes in a millimeter-size QAH-niobium hybrid device. However, non-Majorana mechanisms can also generate similar signatures, especially in disordered samples. Here, we studied similar hybrid devices with a well-controlled and transparent interface between the superconductor and the QAH insulator. When the devices are in the QAH state with well-aligned magnetization, the two-terminal conductance is always half-quantized. Our experiment provides a comprehensive understanding of the superconducting proximity effect observed in QAH-superconductor hybrid devices and shows that the half-quantized conductance plateau is unlikely to be induced by chiral Majorana fermions in samples with a highly transparent interface.

opological superconductors (TSCs) are predicted to host Majorana fermions, particles that are their own antiparticles (1-5). These Majorana fermions obey non-Abelian statistics and are promising candidates to form a topological qubit, which is the basis for fault-tolerant topological quantum computation (6-8). TSCs are predicted to appear in a variety of condensed matter quantum systems including strong spin-orbitcoupled semiconductor-SC hybrid devices (9, 10), fractional quantum Hall (QH) systems at filling factor v = 5/2 (11, 12), spinless $p_x + ip_y$ SCs such as Sr₂RuO₄ (2, 13), hybrid topological insulator (TI)-SC devices (9), integer QH insulators covered by a conventional s-wave SC (14), and thin films of transition metal dichalcogenides (15, 16). Theoretical work has predicted a chiral TSC phase when a quantum anomalous Hall (QAH) insulator, a zeromagnetic field manifestation of the integer QH effect (17, 18), is coupled to an s-wave SC (14, 19).

The QAH effect has been experimentally demonstrated in thin films of magnetically doped TI (18, 20-22). He *et al.* (23) recently reported a half-quantized plateau in the two-terminal conductance $\sigma_{1,2}$ converted from resistance measured across a millimeter-size QAH-Nb hybrid structure and interpreted the half-quantized $\sigma_{1,2}$ plateau during magnetization reversal as a "distinct signature" of one-dimensional chiral Majorana edge modes (CMEMs) (19), Alternative interpre-

¹Department of Physics, Pennsylvania State University, University Park, PA 16802, USA. ²Faculty for Physics and Astronomy (EP3), University of Würzburg, Am Hubland, D-97074 Würzburg, Germany. ³Institute for Topological Insulators, Am Hubland, D-97074 Würzburg, Germany. *These authors contributed equally to this work. †Corresponding author. Email: mhc2@psu.edu (M.H.W.C.);

nxs16@psu.edu (N.S.); cxc955@psu.edu (C.-Z.C.).

tations, however, are also possible. For example, Huang et al. (24) and Ji and Wen (25) theoretically discussed two different scenarios in which a $\sigma_{1,2} = 0.5e^2/h$ plateau (where *e* is the elementary charge and h is the Planck constant) can arise without invoking the Majorana physics. Huang et al. considered the percolation of QAH edges induced by magnetic disorder in the QAH insulator as an alternative origin for the $\sigma_{1,2} = 0.5e^2/h$ plateau. Ji and Wen argued that the $\sigma_{1,2}$ = $0.5e^2/h$ plateau can arise if the SC layer provides good electrical contact to the chiral edge modes of the QAH insulator. In other words, the local equilibrium between the chiral edge modes of the QAH insulators and the SC strip ensures that the total resistance is the series resistance of two separate QAH regions, each with h/e^2 resistance (26).

Here, we studied the effect of contact transparency in the appearance of the $\sigma_{1,2}$ = $0.5e^2/h$ plateau. To this end, we fabricated magnetic TI-SC hybrid devices, an example of which is shown in Fig. 1, A and B. Our device consists of a superconducting Nb strip (width ~20 µm) covering the entire width of the QAH layer on the left, a configuration similar to that in (23), and a narrow Nb finger (width ~200 nm) on the right (Fig. 1, A and B). The QAH sample in this device is a sandwich of 3QL Cr-doped (Bi, Sb)₂Te₃ / 5QL (Bi, Sb)₂Te₃ / 3QL Cr-doped (Bi, Sb)₂Te₃, where QL stands for quintuple layer (27). Our device was designed such that (i) the contact transparency between the magnetic TI and SC layers can be characterized using a differential conductance measurement on the QAH-Nb finger junction (28); (ii) the possible existence of the CMEMs can be investigated by analyzing the two-terminal conductance $\sigma_{1,2}$ deduced from resistance measured across the QAH-Nb strip device (19, 23). Furthermore, our QAH film (i.e., magnetic TI) can be tuned to the metallic state using the back-gate voltage V_g . This allows us to probe the Andreev reflection involved in the magnetic TI-SC hybrid device through the entire phase diagram-that is, as a function of the chemical potential (tuned by V_{α}) and the external magnetic field. When the QAH layer is tuned into the metallic phase, we observed a strong enhancement of the zero-bias electrical conductance, nearly twice (~180%) the normal-state conductance presumably induced by Andreev reflection. The observation of Andreev reflection in our junction is strong evidence for the induced superconducting pair potential in the magnetic TI laver and allows us to study the effect of a transparent interface on the two-terminal conductance $\sigma_{1,2}$ in the QAH-SC hybrid structure. When the magnetic TI is in the QAH regime, the differential conductance is dominated by the density of state modulation (i.e., breakdown) of the QAH effect. When the QAH and SC layers are strongly coupled, as demonstrated by our differential conductance data, σ_{12} is always half-quantized when the magnetization is well aligned. Our conclusions are supported by measurements on ~30 devices (29).

Figure 1C shows the temperature dependence of the Nb finger and the Nb strip resistance. The Nb finger becomes superconducting below its critical temperature $T_{\rm c.finger} \sim 5$ K. The critical temperature of the Nb strip $T_{\rm c,strip}$ is ~8.6 K. Because we are using a two-terminal technique to measure the resistance (between electrodes 8a and 8b in Fig. 1A), the normal leads contribute ~40 ohms to the total resistance, which has been subtracted. Figure 1D plots the magnetic field $(\mu_0 H)$ dependence of the resistances of the Nb finger and the Nb strip. The Nb strip has an upper critical field $\mu_0 H_{\rm c2,strip}$ ~ 2.9 T. Shown in Fig. 1, E and F, are the $\mu_0 H$ dependence of the longitudinal resistance (conductance) ρ_{xx} (σ_{xx}) and the Hall resistance (conductance) $\rho_{yx}(\sigma_{xy})$ at $V_{\rm g}$ = $V_{\rm g}^{0}$ = +42 V and T = 30 mK, where typical QAH characteristics, quantized ρ_{ux} (σ_{xu}) accompanied by vanishing ρ_{xx} (σ_{xx}), are observed. Because the ρ_{xx} peak value during magnetization reversal is comparable to the quantized ρ_{yx} value, the zero-Hall conductance $\sigma_{xy} = 0$ plateau [i.e., Chern number C = 0phase (30)] is not observable. The $\sigma_{xy} = 0$ plateau is usually observed in thinner, uniformly doped QAH samples with a larger ρ_{xx}

We characterized the interface transparency of the magnetic TI-Nb finger junction by measuring its differential conductance, which is related to the probabilities of the Andreev reflection (AR) and the normal reflection (NR) across the interface. Figure 2, A and B, shows the differential upstream conductance $\sigma_{\rm U} = dI_{6.8}/dV_{7.8}$ and the downstream conductance $\sigma_{\rm D} = dI_{6.8}/dV_{9.8}$, where the subscript

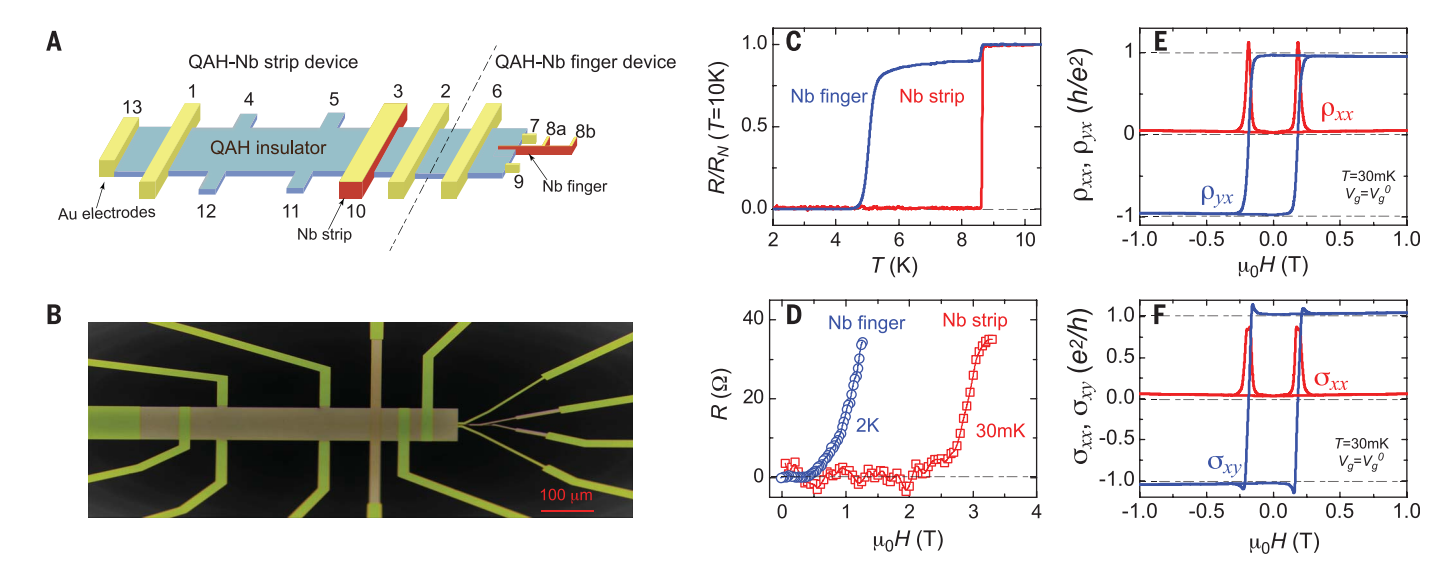


Fig. 1. QAH-Nb device and characterizations. (**A**) Schematic of the device consisting of a QAH insulator layer, a Nb strip, and a Nb finger. The Nb finger is used to characterize the magnetic TI-Nb contact transparency, whereas the Nb strip is used to study the two-terminal conductance $\sigma_{1.2}$ across the QAH-Nb structure. (**B**) Optical microscope image of the device. (**C**) Temperature dependence of the normalized resistance of the Nb finger and Nb strip. The drop

in the resistance of the Nb finger at $T\sim 8.6$ K is associated with a superconducting transition of the Nb section with a larger width ($\sim 4~\mu m$) in the device; see (B) and the inset of Fig. 2A. (**D**) $\mu_0 H$ dependence of the resistance of the Nb finger and Nb strip. (**E** and **F**) The four-terminal longitudinal and Hall resistance (ρ_{xx} and ρ_{yx}) (E) and their corresponding longitudinal and Hall conductance (σ_{xx} and σ_{xy}) (F) as a function of $\mu_0 H$ measured at $V_g = V_g{}^0 = +42$ V and T=30 mK.

numbers correspond to the electrodes shown in Fig. 1A, at different magnetic fields. σ_{IJ} and $\sigma_{\!\scriptscriptstyle D}$ are normalized by their respective values at $T > T_{c,\text{finger}}$ (i.e., $\sigma_{6\text{K}}$). For $V_g = V_g^0$, the differential conductance is determined by an interplay between AR and NR at the interface, as well as the breakdown of the QAH system (33-35): the breakdown of the QAH state turns out to be the dominant contribution in our samples (see fig. S3). On the other hand, σ_{U} (σ_D) is a better probe of the AR/NR ratio when the magnetic TI is in its metallic phase, as discussed below. To characterize the magnetic TI-Nb interface transparency, we applied a negative $V_g = -50 \text{ V}$ to reach the metallic phase of the magnetic TI. At zero magnetic field, we observed an enhancement of the zero-bias conductance approaching 180% of its high-temperature value, revealing a highly transparent magnetic TI-SC interface. Remarkably, although the superconductivity in the Nb finger is suppressed for $\mu_0 H > 0.5 \text{ T}$ (Fig. 1B and fig. S1E), the magnetic TI-Nb contact transparency is unaffected (Fig. 2, A and B). For $\mu_0 H$ larger than the coercive field ($\mu_0 H_c \sim 0.06 \text{ T}$) of the magnetic TI layer at T = 2 K, zero-bias σ_U is slightly reduced and zero-bias $\sigma_{\!\scriptscriptstyle D}$ is slightly increased. The reduction of σ_U and enhancement of σ_D are likely results of the magnetization reversal in the magnetic TI layer around the $\mu_0 H_c$ regime (see fig. S4).

In our experiment, it is difficult to extract accurately the voltage drop across the magnetic TI-Nb junction because a large portion of the voltage drop appears across the resist-

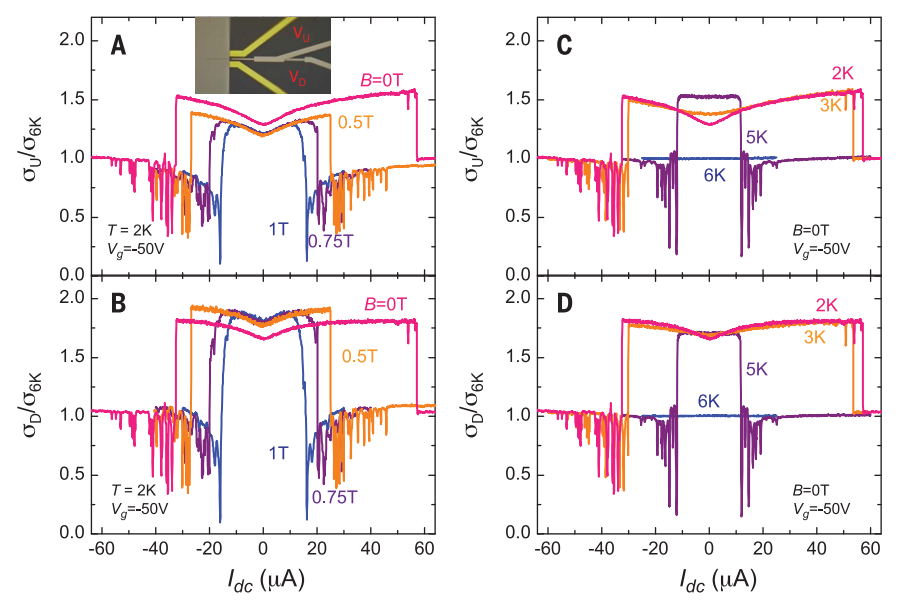


Fig. 2. Contact transparency in the magnetic TI-Nb finger device. (**A** and **B**) The differential upstream conductance $\sigma_{\rm U} = dI_{\rm 6.8}/dV_{\rm 7.8}$ (A) and the downstream conductance $\sigma_{\rm D} = dI_{\rm 6.8}/dV_{\rm 9.8}$ (B) of the magnetic TI-Nb finger junction normalized by their high-temperature ($T > T_{\rm c.finger}$) values $\sigma_{\rm GK}$, measured at different values of $\mu_{\rm O}H$ and T = 2 K. Inset of (A) shows a magnified optical image of the magnetic TI-Nb finger device. (**C** and **D**) The normalized $\sigma_{\rm U}$ (C) and $\sigma_{\rm D}$ (D) measured at different temperatures and zero magnetic field. The excitation current $I_{\rm ac}$ is 10 nA.

ive part of the magnetic TI layer (29). Therefore, we plot the differential conductance as a function of the dc current, $I_{\rm dc}$, rather than the dc voltage, $V_{\rm dc}$. Furthermore, the enhancement in $\sigma_{\rm U}$ ($\sigma_{\rm D}$) may be a result of the combined contribution of the AR process across the magnetic TI-Nb interface and the metal-to-

superconductor transition induced by the critical current of the Nb finger. We also note that the slight reduction of σ_U (σ_D) close to zero bias (i.e., the small zero-bias conductance dip) observed in Fig. 2 is a result of the interplay between the AR and NR at the interface, as predicted by the Blonder, Tinkham,

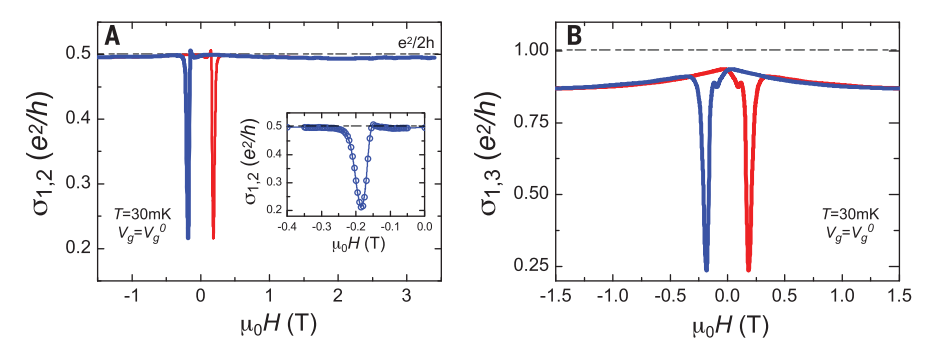


Fig. 3. Two-terminal conductance $\sigma_{1,2}$ across the QAH-Nb strip device. (A) $\mu_0 H$ dependence of $\sigma_{1,2} = dl_{13,6}/dV_{1,2}$ measured at $V_g = V_g^{-0} = +42$ V and T = 30 mK. $\sigma_{1,2} \sim 0.5e^2/h$ for the entire $\mu_0 H$ range when the magnetization is well aligned. No change in $\sigma_{1,2}$ is observed when the Nb strip transitions from the superconducting state to the normal state ($\mu_0 H > \mu_0 H_{c2.strip} \sim 2.6$ T). Inset magnifies the $\mu_0 H$ axis during the magnetization reversal process. (B) $\mu_0 H$ dependence of two-terminal conductance $\sigma_{1,3} = dl_{13,6}/dV_{1,3}$. $\sigma_{1,3}$ approaches $\sim e^2/h$ for $|\mu_0 H| > \mu_0 H_c$, indicating good contact transparency between the Nb strip and the QAH sample. The excitation current l_{ac} is 1 nA. Blue and red curves represent the process for decreasing and increasing $\mu_0 H$, respectively.

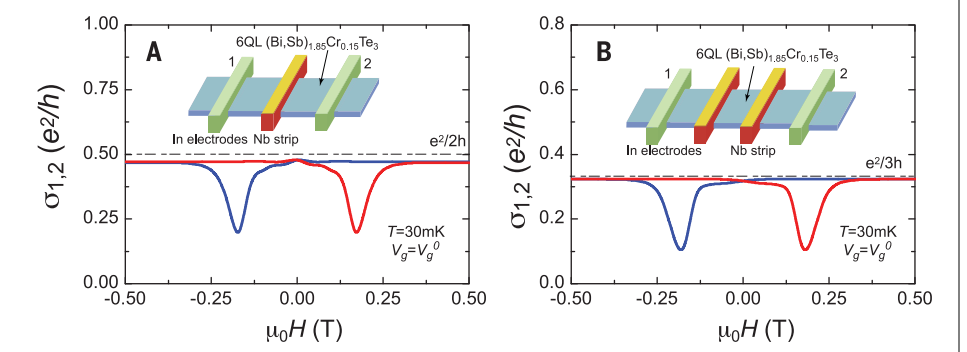


Fig. 4. Two-terminal conductance $\sigma_{1,2}$ in 6QL uniformly doped QAH-Nb strip devices. (A) μ_0H dependence of $\sigma_{1,2}$ measured across one Nb strip stacked on a 6QL (Bi, Sb)_{1,85}Cr_{0,15}Te₃ QAH sample at $V_g = V_g^0$ and T = 30 mK. (B) Same as (A) for two Nb strips. Insets show the corresponding device configurations. With increasing the number (n) of Nb strips, the corresponding $\sigma_{1,2}$ plateau decreases as $\sigma_{1,2} \sim e^2/(n+1)h$. The excitation current I_{ac} is 1 nA. Blue and red curves represent the process for decreasing and increasing μ_0H , respectively.

and Klapwijk (BTK) model for a normal metalsuperconductor junction with a nonzero barrier height (36). To confirm that the sharp zero-bias conductance peak is indeed a result of the AR process at the interface, we studied the temperature dependence of $\sigma_U(\sigma_D)$ versus $I_{\rm dc}$ in Fig. 2, C and D, where we observed a featureless $\sigma_{\rm U}$ ($\sigma_{\rm D}$) at $T=6~{\rm K}>T_{\rm c,finger}.$ We note that at T = 6 K, the Nb finger is no longer superconducting (Fig. 1C), and thus the differential conductance is a sum of the contributions from the NR at the interface and the resistive part of the magnetic TI film. Therefore, the zero-bias conductance at T =6 K takes the same value as that of the highbias regime for $T \le 5$ K, consistent with the AR picture for normal metal-superconductor junctions (29, 36, 37).

Our experimental observations reveal the presence of a highly transparent interface between the magnetic TI and Nb finger

throughout the $\mu_0 H$ range of interest (0 T < $\mu_0 H$ < 1 T). Because the Nb finger and the Nb strip were deposited onto the QAH devices simultaneously, we expect the interface transparency across the magnetic TI-Nb junction to be similar for the strip and the finger. The transparent interface and the chiral nature of the edge modes in the QAH regime are expected to ensure that an electron propagating along the wide Nb strip will quickly become an equal mixture of electrons and holes (28)

Our QAH-SC hybrid device (minus the Nb finger) shown in Fig. 1, A and B, is similar to the device used in (23). A $\sigma_{1,2} \sim 0.5e^2/h$ plateau during the magnetization reversal ($\sim \mu_0 H_c$) followed by a $\sigma_{1,2} \sim e^2/h$ plateau for the $\mu_0 H_c < |\mu_0 H| < \mu_0 H_{c2,strip}$ regime is reported in (23). These measurements were interpreted as induced by the presence of the CMEMs; the transition from the $\sigma_{1,2} = e^2/h$ plateau to

the $\sigma_{1,2} = 0.5e^2/h$ plateau was attributed to a topological phase transition in the TSC state from N = 2 to N = 1, where N denotes the number of CMEMs (14, 19). In the same structure, an extremely small two-terminal conductance $\sigma_{1,3}$, measured between the Nb strip and the QAH sample, for $\mu_0 H_c < |\mu_0 H| < \mu_0 H_{c2.strip}$ was also reported (23). The small value of $\sigma_{1.3}$ in this $\mu_0 H$ range indicates that the Nb layer is likely decoupled from the QAH sample, and hence the $\sigma_{1,2} = e^2/h$ plateau may be a result of poor electrical contact between the QAH insulator and the Nb layers; in that case, there is no proximity-induced superconductivity and no AR at the QAH-Nb interface (23, 25). We note that the observation of $\sigma_{1,2}$ = $0.5e^2/h$ in the QAH insulator phase is not unusual (24, 25). Indeed, a normal metal (e.g., gold) overlaying the two edges of the QAH sample will give rise to such a quantization in $\sigma_{1,2}$ (26).

Our results from the QAH-SC strip devices can be explained without resorting to Majorana physics. Figure 3A displays the μ_0H dependence of the two-terminal conductance $\sigma_{1,2}$ for $V_g = V_g^0 = +42 \text{ V}$ of our device. In contrast to (23), we observed that $\sigma_{1,2} = dI_{13,6}/dV_{1,2}$ $0.5e^2/h$ over the entire range of the magnetic field except in the μ_0H range, when the magnetization of the sample is being reversed near $\mu_0 H_c$. In this range, $\sigma_{1,2}$ drops to ~0.21 e^2/h . Specifically, no change in $\sigma_{1,2}$ is observed when $\mu_0 H$ is increased across the critical field of the Nb strip; that is, $\mu_0 H_{\rm c2,strip} \sim 2.9$ T (Fig. 1D). We also measured $\sigma_{1,3} = dI_{13,6}/dV_{1,3}$, the conductance between the Nb strip and the QAH sample (Fig. 3B). We found that $\sigma_{1,3} \sim e^2/h$ in the entire $|\mu_0 H| > \mu_0 H_c$ range, indicating that the Nb strip is strongly coupled to the QAH sample, leading to the equilibrium of chemical potentials between chiral edge modes of the QAH sample and bulk Nb layer (25). This behavior is what one would expect if a normal metal were used instead of the Nb strip. For $\mu_0 H > \mu_0 H_{\rm c2,strip}$, the Nb strip turns into the normal state, hence $\sigma_{1,2}$ remains half-quantized. We have also studied 9QL V-doped TI samples, which were previously shown to exhibit perfect QAH effect (35, 38-40) and signatures of axion electrodynamics (38). The devices were patterned using an optical lithography process and used MoRe as the SC strip. We again observed the $\sigma_{1,2} \sim 0.5e^2/h$ plateau for the entire $\mu_0 H$ region with well-aligned magnetization (see fig. S8).

The existence of the zero–Hall conductance plateau with the C=0 phase in a QAH sample was claimed as a prerequisite for the observation of the N=1 TSC phase (23). The transition from the C=0 (i.e., N=0) phase to the C=1 (i.e., N=2) phase is given in (23) [citing (19)] as the key evidence for the existence of the N=1 TSC phase. We note, however, that the theoretical calculations in

(19) treated the superconductor strip merely as the "source" of the small energy gap while overlooking the fact that the superconductor strip also serves as an "electrical short" for the QAH device.

Our results, on the other hand, show that the $\sigma_{1,2} = e^2/h$ plateau in the C = 1 phase is very likely a result of decoupling of the QAH insulator from the Nb layer. Hence, it is not predicated upon the existence of a TSC phase with N = 2. To exclude the possibility that the $\sigma_{1,2} \sim 0.5e^2/h$ plateau observed in our QAH sandwich sample may be caused by the absence of the zero-Hall conductance plateau (i.e., the C = 0 phase), we carried out measurements on QAH samples with the C = 0phase. We fabricated two 6QL Cr-doped (Bi, Sb)₂Te₃ samples similar to the ones used in (23). Next, we scratched both samples into millimeter-size Hall bar structures (0.5 mm × 1 mm) and then sputtered Nb strips onto the samples with a mask. We measured $\sigma_{1,2}$ across one and two Nb strips. The value of $\sigma_{1,2}$ for one Nb strip sample (Fig. 4A) is similar to that measured in the QAH sandwich sample (Fig. 3A). Therefore, the existence or the nonexistence of the zero-Hall conductance plateau in QAH samples does not change our findings; specifically, the $\sigma_{1,2} \sim 0.5e^2/h$ plateau is observed for the entire $\mu_0 H$ region with wellaligned magnetization. We also studied the V-doped TI/TI/Cr-doped TI QAH sandwich samples, in which a well-established C = 0insulating phase (i.e., the axion insulator state) emerges (41, 42). Here, we also observed the $\sigma_{1,2} \sim 0.5e^2/h$ plateau for the entire $\mu_0 H$ region with well-aligned magnetization (see fig. S7). To better understand the relation between $\sigma_{1,2}$ and the coupling of the SC layer to the chiral edge modes, we measured $\sigma_{1,2}$ across a 6QL Cr-doped (Bi, Sb)₂Te₃ QAH sample with two Nb strips. We observed $\sigma_{1,2} \sim e^2/3h$ for the entire well-aligned $\mu_0 H$ regimes (Fig. 4B). The value of the $\sigma_{1,2}$ plateau decreases with an increasing number of Nb strips (n), specifically $\sigma_{1,2} \sim e^2/(n+1)h$, which indicates that the total two-terminal resistance $\rho_{1,2}$ is a series resistance of (n+1) QAH sections, each contributing h/e^2 (26).

Our results demonstrate that if the SC layer is strongly coupled to the QAH sample, the two-terminal conductance $\sigma_{1,2}$ is half-quantized throughout the magnetic field range where the magnetization is well aligned. The agreement among the data obtained from the various QAH samples with different geometries demonstrates the robustness, reproducibility, and generality of the presented phenomena. Therefore, we conclude that the observation of $\sigma_{1,2} \sim 0.5e^2/h$ plateau alone is not sufficient evidence for the existence of chiral Majorana edge modes and the N=1 TSC phase in the millimeter-size QAH-SC hybrid structures.

REFERENCES AND NOTES

- 1. E. Majorana, Nuovo Cim. 14, 171-184 (1937).
- N. Read, D. Green, Phys. Rev. B 61, 10267–10297 (2000).
- C. W. J. Beenakker, Annu. Rev. Condens. Matter Phys. 4, 113–136 (2013).
- 4. J. Alicea, Rep. Prog. Phys. 75, 076501 (2012).
- 5. X. L. Qi, S. C. Zhang, Rev. Mod. Phys. 83, 1057-1110 (2011).
- 6. A. Y. Kitaev, Ann. Phys. 303, 2-30 (2003).
- 7. F. Wilczek, Nat. Phys. 5, 614-618 (2009).
- C. Nayak, S. H. Simon, A. Stern, M. Freedman, S. Das Sarma, Rev. Mod. Phys. 80, 1083–1159 (2008).
- 9. L. Fu, C. L. Kane, Phys. Rev. Lett. 100, 096407 (2008).
- R. M. Lutchyn, J. D. Sau, S. Das Sarma, Phys. Rev. Lett. 105, 077001 (2010).
- 11. G. Moore, N. Read, Nucl. Phys. B 360, 362-396 (1991).
- 12. A. Stern, Nature **464**, 187–193 (2010).
- 13. A. P. Mackenzie, Y. Maeno, Rev. Mod. Phys. 75, 657-712 (2003)
- 14. X. L. Qi, T. L. Hughes, S. C. Zhang, Phys. Rev. B 82, 184516 (2010).
- N. F. Q. Yuan, K. F. Mak, K. T. Law, *Phys. Rev. Lett.* 113, 097001 (2014).
- Y. T. Hsu, A. Vaezi, M. H. Fischer, E. A. Kim, Nat. Commun. 8, 14985 (2017).
- 17. F. D. M. Haldane, Phys. Rev. Lett. 61, 2015-2018 (1988).
- 18. C. Z. Chang et al., Science 340, 167-170 (2013).
- J. Wang, Q. Zhou, B. Lian, S. C. Zhang, *Phys. Rev. B* 92, 064520 (2015).
- 20. C. Z. Chang et al., Nat. Mater. 14, 473-477 (2015)
- 21. J. G. Checkelsky et al., Nat. Phys. 10, 731-736 (2014).
- 22. X. Kou et al., Phys. Rev. Lett. 113, 137201 (2014).
- 23. Q. L. He et al., Science 357, 294-299 (2017).
- 24. Y. Y. Huang, F. Setiawan, J. D. Sau, Phys. Rev. B 97, 100501 (2018).
- 25. W. Ji, X. G. Wen, Phys. Rev. Lett. 120, 107002 (2018).
- 26. C. Z. Chang et al., Phys. Rev. Lett. 115, 057206 (2015).

- J. Jiang et al., arXiv 1901.07611 [cond-mat.mes-hall] (28 January 2019).
- 28. G. H. Lee et al., Nat. Phys. 13, 693-698 (2017).
- 29. See supplementary materials.
- 30. J. Wang, B. Lian, S. C. Zhang, Phys. Rev. B 89, 085106 (2014).
- 31. X. Kou et al., Nat. Commun. 6, 8474 (2015).
- 32. Y. Feng et al., Phys. Rev. Lett. 115, 126801 (2015).
- 33. M. Kawamura et al., Phys. Rev. Lett. 119, 016803 (2017).
- 34. E. J. Fox et al., Phys. Rev. B **98**, 075145 (2018). 35. M. Götz et al., Appl. Phys. Lett. **112**, 072102 (2018).
- G. E. Blonder, M. Tinkham, T. M. Klapwijk, Phys. Rev. B 25, 4515–4532 (1982).
- 37. M. Tinkham, Introduction to Superconductivity (McGraw-Hill, 1996).
- 38. S. Grauer et al., Phys. Rev. Lett. 118, 246801 (2017).
- 39. M. Winnerlein et al., Phy. Rev. Mater. 1, 011201 (2017).
- 40. S. Grauer et al., Phys. Rev. B 92, 201304 (2015).
- 41. D. Xiao et al., Phys. Rev. Lett. 120, 056801 (2018).
- 42. M. Mogi et al., Sci. Adv. 3, eaao1669 (2017).
- C. Z. Chang, Data for "Absence of Evidence for Chiral Majorana Modes in Quantum Anomalous Hall-Superconductor Devices"; https://doi.org/10.7910/DVN/QWQEHT, Harvard Dataverse (2019).

ACKNOWLEDGMENTS

We thank C. X. Liu, K. T. Law, B. Lian, J. Wang, X. Dai, J. Jain, H. Z. Lu, Z. Wang, B. H. Yan, G. H. Lee, Y. L. Chen, K. He, W. J. Ji, Q. K. Xue, and X. D. Xu for helpful discussions. Funding: Supported by ONR grant N-000141512370 and Penn State 2DCC-MIP under NSF grant DMR-1539916 (N.S.); DOE grant DE-FG01-08ER46531 (O.L.); NSF grant DMR-1707340 (M.H.W.C.); NSF-CAREER award DMR-1847811, ARO Young Investigator Program Award W911NF1810198, and an Alfred P. Sloan Research Fellowship (C.-Z.C.); and EU ERC-AG Programs (project 3-TOP and 4TOPS) (C.G. and L.W.M.). Support for transport measurements and data analysis at Penn State is provided by DOE grant DE-SC0019064. Author contributions: N.S., M.H.W.C., and C.-Z.C. conceived and designed the experiment; D.X. and R.X. grew the QAH samples. M.K. fabricated the devices; M.K., J.S., and R.Z. performed the dilution refrigerator measurements; M.K., J.J., F.W., Y.-F.Z. and L.Z. carried out the PPMS transport measurements; C.G. and L.W.M. conceived and designed the experiment done in Würzburg; M.W. grew the QAH samples in Würzburg; K.M.F. and P.M. fabricated the devices and performed the dilution refrigerator measurements in Würzburg; M.K., C.G., N.S., M.H.W.C., and C.-Z.C. wrote the manuscript; all authors contributed to the analysis of the data and the final editing of the manuscript. Competing interests: The authors declare no competing interests. Data and materials availability: All data in the main text and the supplementary materials are available at (43)

SUPPLEMENTARY MATERIALS

science.sciencemag.org/content/367/6473/64/suppl/DC1 Materials and Methods Supplementary Text Figs. S1 to S10

9 April 2019; accepted 7 November 2019 10.1126/science.aax6361

References (44-46)



Absence of evidence for chiral Majorana modes in quantum anomalous Hall-superconductor devices

Morteza Kayyalha, Di Xiao, Ruoxi Zhang, Jaeho Shin, Jue Jiang, Fei Wang, Yi-Fan Zhao, Run Xiao, Ling Zhang, Kajetan M. Fijalkowski, Pankaj Mandal, Martin Winnerlein, Charles Gould, Qi Li, Laurens W. Molenkamp, Moses H. W. Chan, Nitin Samarth and Cui-Zu Chang

Science **367** (6473), 64-67. DOI: 10.1126/science.aax6361

Looking for chiral Majoranas

Čhiral Majorana modes have been predicted to exist in heterostructures consisting of a quantum anomalous Hall insulator and a superconductor. Kayyalha et al. fabricated more than 30 such samples and used transport measurements to look for signatures of the Majorana modes. The data indicated that the transport signatures previously thought to be associated with Majorana physics could, in their samples, be explained using a more mundane mechanism.

Science, this issue p. 64

ARTICLE TOOLS http://science.sciencemag.org/content/367/6473/64

SUPPLEMENTARY http://science.sciencemag.org/content/suppl/2019/12/30/367.6473.64.DC1

REFERENCES This article cites 45 articles, 6 of which you can access for free

http://science.sciencemag.org/content/367/6473/64#BIBL

PERMISSIONS http://www.sciencemag.org/help/reprints-and-permissions

Use of this article is subject to the Terms of Service